Thermal oxidation of Ru(0001) to RuO2(110) studied with ambient pressure x-ray photoelectron spectroscopy

Diulus, J Trey ; Tobler, Benjamin ; Osterwalder, Jürg ; Novotny, Zbynek

Abstract: The thermal oxidation of Ru(0001) has been extensively studied in the surface science community to determine the oxidation pathway towards ruthenium dioxide (RuO2(110)), improving the knowledge of Ru(0001) surface chemistry. Using time-lapsed ambient-pressure x-ray photoelectron spectroscopy (APXPS), we investigate the thermal oxidation of single-crystalline Ru(0001) films toward rutile RuO2(110) in situ. APXPS spectra were continuously collected while the Ru(0001) films were exposed to a fixed O2 partial pressure of 10−2 mbar and the sample temperature was increased stepwise from room temperature to 400 °C. We initially observe the removal of adventitious carbon and subsequent formation of a chemisorbed oxygen overlayer at 250 °C. Further annealing to 300 °C leads to an increase in thickness of the oxide layer and a shift in the Ru–O component of the Ru 3d spectra, indicating the presence of a metastable O–Ru–O trilayer structure. A rapid formation of the RuO2 rutile phase with an approximate thickness of at least 2.6 nm is formed about four minutes after stabilizing the temperature at 350 °C and subsequent annealing to 400 °C, signaled by a distinct binding energy shift in both the Ru 3d and O 1s spectra, as well as quantitative analysis of XPS intensities. This observed autocatalytic oxidation process agrees well with previous theoretical models and experimental studies, and the data provide the unambiguous spectral identification of one proposed metastable precursor required for full oxidation to rutile RuO2(110). Further ex situ characterization of the grown oxide with x-ray photoelectron diffraction confirms the presence of three rotated domains of rutile RuO2(110) and reveals their orientation relative to the substrate lattice.

DOI: https://doi.org/10.1088/1361-6463/abedfd

Journal of Physics D: Applied Physics

PAPER • **OPEN ACCESS**

Thermal oxidation of Ru(0001) to RuO_2(110) studied with ambient pressure x-ray photoelectron spectroscopy

To cite this article: J Trey Diulus *et al* 2021 *J. Phys. D: Appl. Phys.* **54** 244001

OPEN ACCESS
IOP Publishing
Journal of Physics D: Applied Physics
J. Phys. D: Appl. Phys. **54** (2021) 244001 (10pp)
https://doi.org/10.1088/1361-6463/abedfd

Thermal oxidation of Ru(0001) to RuO_2(110) studied with ambient pressure x-ray photoelectron spectroscopy

J Trey Diulus[1,2], Benjamin Tobler[1], Jürg Osterwalder[1] and Zbynek Novotny[1,2,*]

[1] Physics Institute, University of Zürich, 8057 Zürich, Switzerland
[2] Paul Scherrer Institute, 5232 Villigen PSI, Switzerland

E-mail: novotny@physik.uzh.ch

Received 29 October 2020, revised 2 March 2021
Accepted for publication 11 March 2021
Published 30 March 2021

Abstract

The thermal oxidation of Ru(0001) has been extensively studied in the surface science community to determine the oxidation pathway towards ruthenium dioxide (RuO_2(110)), improving the knowledge of Ru(0001) surface chemistry. Using time-lapsed ambient-pressure x-ray photoelectron spectroscopy (APXPS), we investigate the thermal oxidation of single-crystalline Ru(0001) films toward rutile RuO_2(110) *in situ*. APXPS spectra were continuously collected while the Ru(0001) films were exposed to a fixed O_2 partial pressure of 10^{-2} mbar and the sample temperature was increased stepwise from room temperature to 400 °C. We initially observe the removal of adventitious carbon and subsequent formation of a chemisorbed oxygen overlayer at 250 °C. Further annealing to 300 °C leads to an increase in thickness of the oxide layer and a shift in the Ru–O component of the Ru 3d spectra, indicating the presence of a metastable O–Ru–O trilayer structure. A rapid formation of the RuO_2 rutile phase with an approximate thickness of at least 2.6 nm is formed about four minutes after stabilizing the temperature at 350 °C and subsequent annealing to 400 °C, signaled by a distinct binding energy shift in both the Ru 3d and O 1s spectra, as well as quantitative analysis of XPS intensities. This observed autocatalytic oxidation process agrees well with previous theoretical models and experimental studies, and the data provide the unambiguous spectral identification of one proposed metastable precursor required for full oxidation to rutile RuO_2(110). Further *ex situ* characterization of the grown oxide with x-ray photoelectron diffraction confirms the presence of three rotated domains of rutile RuO_2(110) and reveals their orientation relative to the substrate lattice.

Supplementary material for this article is available online

Keywords: APXPS, ruthenium dioxide, surface oxidation, thermal oxidation, XPD

(Some figures may appear in colour only in the online journal)

* Author to whom any correspondence should be addressed.

1. Introduction

Ruthenium dioxide (RuO_2) is a promising oxidation catalyst for numerous reactions, specifically low-temperature dehydrogenation of ammonia [1], HCl oxidation [2], and alcohol combustion [3, 4]. RuO_2 has also shown promise in electrocatalysis due to the formation of hydrous RuO_2 [4]. Reactions on well-prepared Ru and RuO_2 surfaces have been extensively studied in surface science as model systems. There is a well-known catalytic pressure gap, where the Ru metal surface is inactive towards CO oxidation at low oxygen partial pressures, but becomes one of the most active catalysts as the oxygen ambient increases [4, 5]. Over *et al* proved that this increase in activity of Ru metal is due to the formation of a RuO_2 film at the surface, allowing for CO molecules to adsorb and react with surface oxygen [6]. Thus, understanding the nature of Ru oxidation is imperative towards understanding reactions on Ru surfaces.

Recent studies have shown that the Ru(0001) surface can be thermally oxidized by annealing the sample in molecular oxygen, forming Ru^{4+} cations in a rutile structure [7, 8]. The stoichiometric (110) surface orientation exposes two kinds of under-coordinated atoms: bridging oxygen (O_{br}) atoms coordinated to two instead of three Ru atoms, and the one-fold coordinatively unsaturated Ru atoms (1f–cus–Ru) coordinated to five instead of six oxygen atoms [6]. The 1f–cus–Ru site is an electron accepting site, while the O_{br} is a hydrogen accepting site, similar to many other rutile transition metal oxides, where the driving factor for surface reactions is rooted in the redox chemistry between these sites [4, 9, 10]. When Ru(0001) is exposed to O_2 in ultra-high vacuum (UHV), the O_2 molecules dissociate without activation, leading to the formation O–Ru bonds more strongly bound than in RuO_2 [4]. STM images during Ru(0001) oxidation at 550 K with a 10^{-5} mbar O_2 partial pressure have displayed evidence of a nucleation and growth mechanism [4, 11]. However, RuO_2 nuclei are only stable after reaching a critical size dependent on oxygen pressure and sample temperature [12]. Before this critical size is reached, formation and decomposition of metastable RuO_2 nuclei takes place concurrently [12–14]. Once a stable nucleus of RuO_2 is formed, it greatly enhances the dissociation of molecular oxygen and the rate of the oxide growth increases rapidly, as it is self-catalyzed by the presence of RuO_2 [12, 14]. It is generally agreed that for a complete oxidation of Ru(0001) to RuO_2(110), elevated temperatures (>550 K) and near ambient pressures of molecular O_2 (>10^{-5} mbar) are required [4].

While the chemistry of reactions on model RuO_2 surfaces has been well studied, few studies have been successful in experimentally determining the pathway for how a thermally grown oxide forms on a pristine Ru(0001) surface [4]. Exposure of Ru(0001) to molecular oxygen at room temperature (RT) leads to various structures of chemisorbed oxygen that mainly include the (2 × 2)-O, (2 × 1)-O, (2 × 2)-3O and (1 × 1)-O phases [4]. Literature has previously proposed from thermal desorption spectra and theory that the formation of an O–Ru–O trilayer or suboxides RuO_x are involved in creating RuO_2 [11, 15]. According to the model suggested by Over and co-workers, the RuO_2(110) active phase coexists with islands of inactive (1 × 1)-O chemisorbed phase [14, 16]. There has been extensive work focusing on studying the oxidation of CO catalyzed by RuO_2(110) at pressures up to 10^{-2} mbar. These studies, summarized in [13], demonstrate the variation of the Ru oxidation state by varying the CO/O_2 ratio. While such studies provide a great deal of information, in particular high-resolution XPS spectra for nearly all known sub-oxide phases of ruthenium, including the sub-surface incorporation of oxygen atoms and information about the spatial distribution of such phases, a complementary *in situ* study showing the transition between different oxide phases and coexistence of such phases during exposure solely to O_2, along with their kinetics of formation, is still lacking in the literature.

A fundamental approach to improve our understanding of oxidation precursors on late transition metal surfaces and their spectral identification is imperative for the heterogeneous catalysis community and can lead to improved catalyst designs [4, 5]. Unfortunately, obtaining chemical state information of intermediate oxides *in situ* has proven difficult. Specifically for Ru, these intermediate oxides are expected to be metastable [15], requiring an experimental design that can collect data quickly while holding one of two variables (either temperature or pressure) constant during oxidation. Prior experiments where the surface was oxidized through specific Langmuir doses, followed by XPS and temperature-programmed desorption spectroscopy measurements under UHV conditions after each dose, provided spectral identification for individual steps during oxidation [11]. However studying the oxidation during a continuous experiment at higher O_2 pressure (10^{-2}) is expected to more closely resemble the oxidation pathway that occurs under reaction conditions.

In this study, we report on the thermal oxidation of single-crystalline Ru(0001) films, *in situ*, during time-lapsed ambient pressure x-ray photoelectron spectroscopy (APXPS) measurements. As-received Ru(0001) films were inserted into an APXPS endstation and annealed stepwise from RT to 400 °C in a constant O_2 partial pressure (p_{O2}) of 1 × 10^{-2} mbar. With quantitative analysis, we calculated the stoichiometry of the formed oxide film and provide evidence for a model pathway of the oxidation of Ru(0001). Furthermore, following oxidation, the formed oxide film structure is verified to be rutile RuO_2(110) through *ex situ* x-ray photoelectron diffraction (XPD) and low-energy electron diffraction (LEED) characterization.

2. Methods

Ru samples were composed of a 200 nm thick Ru(0001) film deposited on a yttria-stabilized-zirconia film on top of a Si(111) substrate [17]. As-received samples were first cleaned *ex situ* in a UV/ozone cleaner [18], followed by thermal annealing in HV (10^{-8} mbar) to 700 °C. The samples were not ion sputter cleaned as this damaged the crystallinity and was not required to remove contaminants. More information

about sputtering damage is provided in the supporting information (SI) section S1. LEED and XPD were utilized to determine the crystallinity of the Ru(0001) films and to ensure that a RuO_2(110) structure was formed after thermal pre-treatment, also shown in the SI. All data presented in sections S1 and S2 of the SI (available online at stacks.iop.org/JPD/54/244001/mmedia), together with the XPD data shown in figure 3, were acquired in a separate UHV instrument described by Greber *et al* [19]. APXPS experiments were carried out using the solid–gas interface chamber (SGIC) endstation at the Swiss Light Source [20]. The SGIC utilizes a Scienta R4000 HiPP-2 ambient pressure electron analyzer attached to the *In Situ* Spectroscopy beamline (X07DB) that is nearly identical as beamline X07DA described by Raabe *et al* in [21]. The beamline uses a double crystal monochromator with a 300–400 μm spot size and an average beam current of 17 μA measured with a photodiode (AXUV100) at a photon energy of 1000 eV [21]. Low-resolution survey spectra were collected with a photon energy of 1000 eV (see figure S8 (SI), together with the photon energy-dependent energy resolution shown in figure S9), while iterative high-resolution Ru 3d + C 1s and O 1s spectra were collected during the thermal oxidation process with a photon energy of 653 eV. Acquisition of Ru + C required 18 s per iteration, while the O 1s region required 24 s, for a total of 42 s for each total iteration.

During oxidation, the high-pressure cell was initially filled with $p_{O2} = 1 \times 10^{-2}$ mbar prior to annealing. The pressure was measured with a combination of three calibrated Baratron® capacitance manometer gauges with pressure detection ranges between 10 and 10^{-3} mbar. Once the pressure was stabilized, the sample was heated up to 350 °C using step sizes of 50 °C. At each step, the temperature was held to collect a series of approximately 20 iterations (14 min) of XPS spectra until 350 °C was reached, where the temperature was held for 70 iterations (49 min). The temperature was then raised to 390 °C for 40 iterations (28 min) followed by a final ramp to 400 °C and then immediately cooled to 70 °C. The heating was performed using an infrared laser diode for irradiating an oxygen-free high-conductivity copper plate in direct contact with the sample and was measured with a Pt100 sensor in direct contact with the laser-heated Cu backplate. Prior to all data collection, the gas cell was flushed with oxygen and outgassed at a temperature of 500 °C for three hours. No contamination was detected other than adventitious carbon (see survey shown in figure S8 of SI).

Fast XPS spectra were acquired using a photon energy of 653 eV at an emission angle of 30° with linearly polarized light, where the polarization vector was aligned with the optical path of the electron spectrometer. The sample was thus irradiated at 60° with respect to the surface normal. Photoelectrons were detected using a pass energy of 20 eV with a fully open analyzer slit. The binding energy scale was calibrated using the Au 4f core level peak position on a polycrystalline gold sample. Spectra were processed using IgorPRO, MATLAB and CasaXPS software packages. The spectra were additionally normalized to align the background intensity below the photoemission peak to the same value.

XPD simulations were performed using the electron diffraction in atomic clusters package [22]. Refer to SI figure S3 showing the XPD pattern obtained from a RuO_2(110) cluster consisting of 1272 atoms (see figure S4) and simulated at a kinetic energy of 973 eV. Applied symmetry operations are mentioned later in the text and a full description of the simulated XPD analysis is provided in the SI.

3. Results and discussion

To monitor the temperature-dependent oxidation of Ru(0001) during exposure to O_2 *in situ* we utilized APXPS. The partial pressure of O_2 (p_{O2}) was set to 1×10^{-2} mbar starting at RT, followed by incremental heating from 100 to 400 °C with step sizes of 50 °C as shown in figure 1(c). The temperature was held at each increment for the length of the collection time needed for sufficient signal-to-noise ratio for both Ru 3d + C 1s and O 1s high-resolution core level spectra. The C 1s core level overlaps with the Ru $3d_{3/2}$ peak, hence the notation Ru 3d + C 1s. Figure 1 shows a heat map of the spectral intensities of O 1s (a) and Ru 3d + C 1s (b) plotted against sequential iterations during *in situ* oxidation of Ru(0001). The temperature corresponding to each iteration (c) is plotted below. There are five key regions of interest during the experiment that we chose to look at more closely with higher resolution and that are denoted with a colored bar on the time axis. Spectra for each temperature interval were averaged and plotted for visual comparison in figures 1(d) and (e), with corresponding colors used for the bars in figures 1(a)–(c).

Already at iterations 90–110 (black curves, 250 °C), we observe adventitious carbon contamination being burned away causing what appears as a slight shift of the combined Ru $3d_{3/2}$ + C peak to lower binding energy, accompanied by an increase in the Ru metal (Ru^0) component in the Ru $3d_{5/2}$ spectrum and of the chemisorbed oxygen component in O 1s as temperature increases. A strong increase in the O 1s at 530 eV heralds the beginning of the oxidation process at 300 °C, and the coexistence of Ru^0 and Ru–O peaks in the Ru 3d core levels at iterations 140–145 (blue curves, 350 °C) shows its progression. Since most of the carbon contamination is burned away, the Ru signal intensity has increased, as is indicated by a faint dark blue color appearing in figure 1(b).

A sudden and significant shift in binding energy for both Ru 3d and O 1s is seen at iteration 150, approximately six minutes after the temperature has stabilized at 350 °C, indicating a dramatic change in the chemical state of the surface from the one seen at iterations 140–145 (blue curves). The surface remains completely stable at 350 °C for 50 iterations (35 min) and continues this stability for an additional 100 iterations (70 min) as the temperature is increased to 390 and 400 °C. Iterations 210–250 (green curves) represent a large portion of this stable region, where a clear satellite peak forms at approximately 282.5 eV, in between the Ru $3d_{5/2}$ and $3d_{3/2}$ peaks, characteristic of RuO_2. The metal component of the Ru 3d spectra becomes negligible, which suggests a film thickness of at least 2.6 nm [4, 23, 24]. After the sample is cooled back to RT, more subtle peak shifts occur for both the Ru–O and cus–Ru

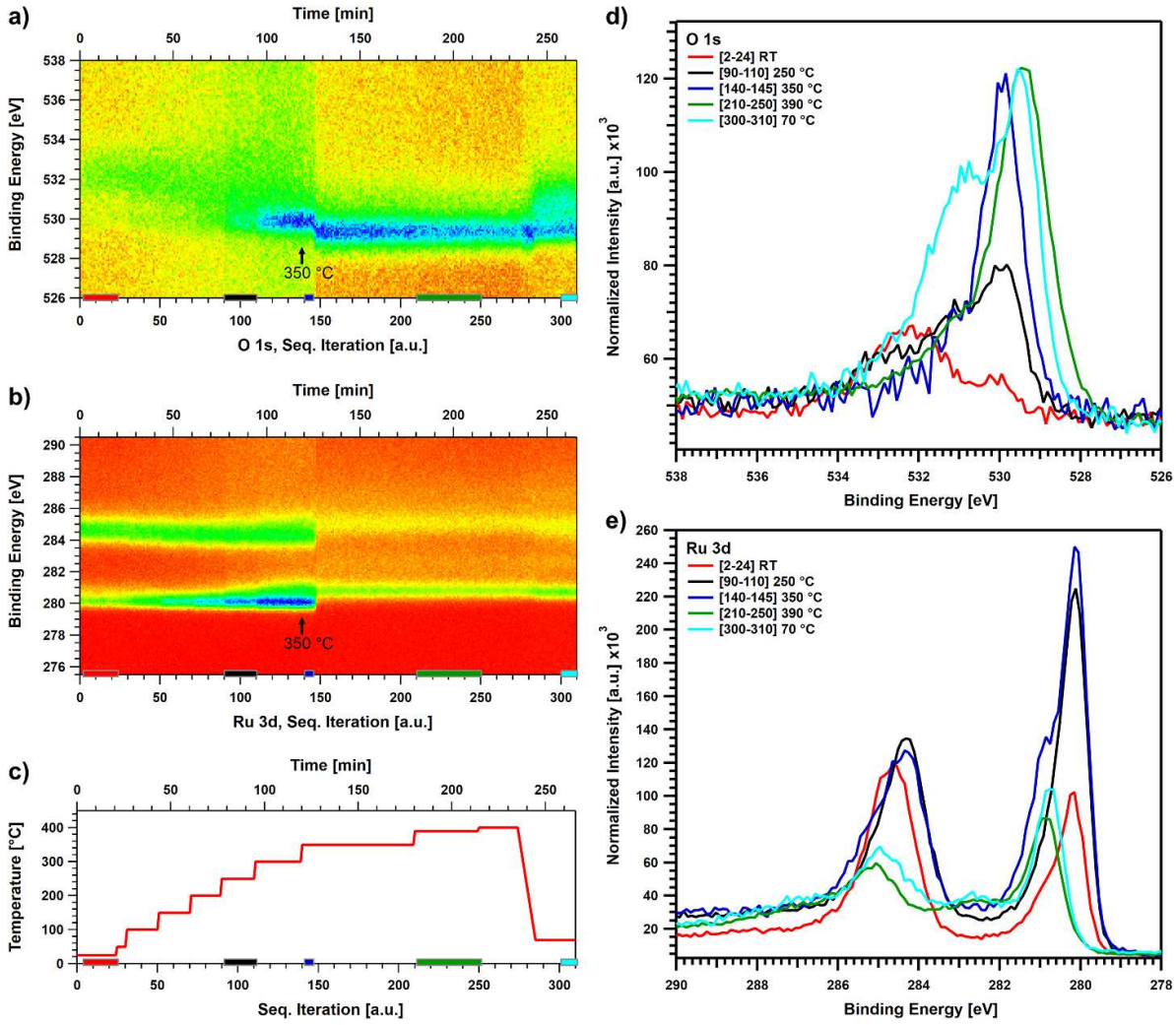

Figure 1. Heat map of O 1s (a) and Ru 3d + C 1s (b) during thermal oxidation of Ru(0001) plotted on a four color scale (red/yellow/green/blue), where red is the minimum intensity and blue is the maximum intensity. Acquisition of Ru + C required 18 s per iteration, while the O 1s region required 24 s, for a total of 42 s for each total iteration. An initial baseline was collected from iterations 2–24. Annealing started at iteration 25 and increased stepwise to 400 °C as depicted by the temperature vs. iteration plot (c). Arrows in (a) and (b) depict when the temperature is stabilized at 350 °C, highlighting a short induction period of approximately six min before a drastic transition at iteration 150. Regions of collected spectra were averaged at five temporal regions during data collection and plotted against each other for O 1s (d) and Ru 3d + C 1s (e). Each region is denoted in (a)–(c) by a color bar on the *x*-axis in the same color as the spectra in (d) and (e). Each spectrum was normalized by the number of iterations used for each section.

3d spectra, seen in iterations 300–310 (cyan curves, 70 °C), as water and adventitious carbon species adsorb to the surface.

In order to analyze the XPS data quantitatively, peak fitting was applied to the averaged spectra shown in figures 1(d) and (e). All XPS peak fitting parameters are tabulated in table S1 (SI). Figure 2(a) depicts the peak fits for Ru 3d + C 1s core levels for each temperature region. Initially, at RT (iterations 2–24), a significant amount of carbon (green curve, 284.7 eV) on the surface causes the putative Ru $3d_{3/2}$ peak to be larger than the $3d_{5/2}$, offsetting the expected 3:2 spin-orbit branching ratio. The Ru $3d_{5/2}$ (dark blue, 280.1 eV) and $3d_{3/2}$ (red, 284.3 eV) peaks are accompanied by corresponding Ru–O $3d_{5/2}$ (gold, 280.8 eV) and $3d_{3/2}$ (light blue, 285.0 eV) peaks due to exposure to atmosphere prior to sample transfer [25]. Once most of the carbon is burned away at 250 °C (iterations 90–110), a slight 0.2 eV shift to lower binding energy (BE) occurs in the Ru–O metal peaks, while the Ru^0 peaks remain at the same positions. This shift suggests the presence of an oxide covered surface, consistent with Ru coordinated to 2 O atoms [Ru(I)–(2O)] proposed by the 0.54 eV separation between the Ru–O and Ru^0 peaks [25, 26]. The intensities of both the Ru^0 and Ru–O peaks also increase as the surface contamination is removed. At 350 °C (iterations 140–145), the Ru–O peaks now experience a slight 0.3 eV shift to higher BE, while the Ru^0 peaks continue to remain at the same position. In figure 1(b), we see that immedately after iteration 145, the Ru 3d peaks shift drastically. This suggests that the spectra for iterations 140–145 denote the presence of a metastable precursor required for the formation of RuO_2. It has been extensively discussed in literature, that the formation of a (1 × 1)-O overlayer and the subsequent formation of metastable trilayer(s) precedes the oxide growth [15, 26].

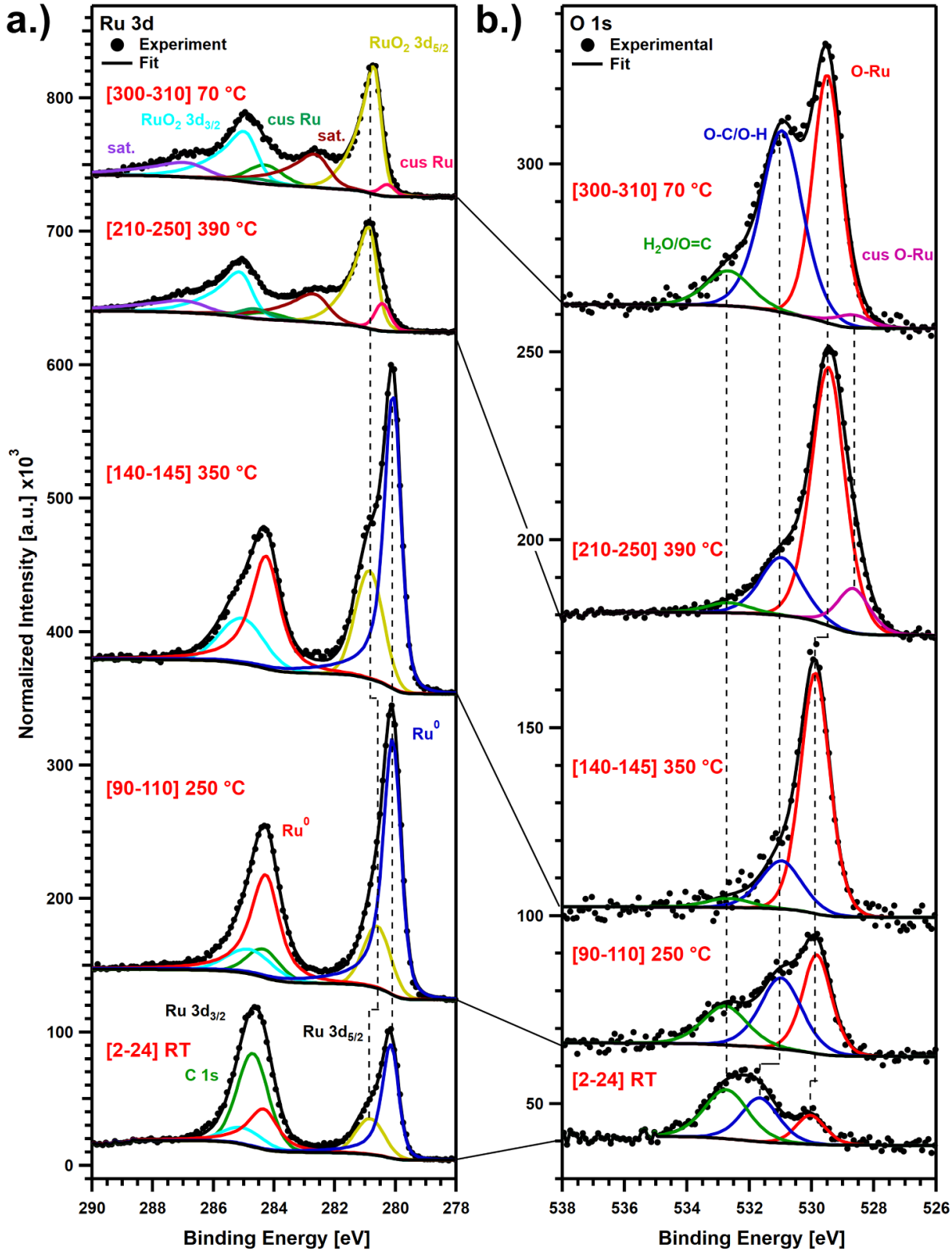

Figure 2. Fitted high resolution Ru 3d + C 1s (a) and O 1s (b) XPS spectra showing regions from each temperature setting. Fitting parameters are included in table S1.

After the sudden change at iteration 150 (350 °C) and upon further annealing at 390 °C (iterations 210–250), the spectra remain unchanged. The metal Ru^0 peak has completely disappeared and the satellite peaks of $3d_{5/2}$ (dark red, 282.5 eV) and $3d_{3/2}$ (purple, 286.7 eV) appear due to core hole screening, which are characteristic of rutile RuO_2 [27]. The Ru 3d main peaks now display a more significant asymmetric tail, consistent with prior literature and attributed to plasmon screening

effects [16]. Moreover, a weak lower energy peak is formed, which corresponds with coordinatively unsaturated (cus) Ru (light red, 280.4 eV). Density functional theory (DFT) calculations have confirmed this −0.35 eV shift of cus–Ru relative to bulk Ru [26]. After cooling down to 70 °C (iterations 300–310), no noticeable change occurs compared to the spectra at 390 °C other than the increase of adsorbed carbon and additional contamination of the surface from the residual hydrogen and water vapor present in the high-pressure cell.

Figure 2(b) depicts the peak fits for O 1s core levels at each temperature interval. At RT (iterations 2–24), adventitious carbon or hydroxyls (blue, 531.7 eV) and adsorbed water or carbonyls (green, 532.7 eV) are the primary contributions, with a small O–Ru component (red, 530.0 eV) [26, 28]. While the sample is being constantly exposed to $p_{O2} = 1 \times 10^{-2}$ mbar O_2, the density is too low to produce a gas phase O_2 peak. After annealing to 250 °C (iterations 90–110) we see a marked increase in O–Ru, consistent with the Ru 3d spectra and confirming the removal of some adventitious contamination. This removal of carbon is what causes a slight 0.2 eV shift to lower BE for the O–Ru peak (529.8 eV). An additional 0.7 eV peak shift to lower binding energy for the adventitious carbon related O-C peak (531.0 eV) is seen, although this is most likely due to the removal and possible combustion of some adventitous species that we cannot further specify. It should be emphasized that, with a photon energy of 653 eV, O 1s photoelectrons appear with relatively low kinetic energies of around 120 eV which makes these spectra particularly surface sensitive. At 350 °C (iterations 140–145) nearly all adventitious contamination is removed and the O–Ru peak becomes the primary component.

Further annealing to 390 °C (iterations 210–250) leads to a significant 0.4 eV shift to lower binding energy for the O–Ru peak, consistent with lattice O in RuO_2 (529.5 eV) [23, 26]. The presence of a satellite peak in the O 1s has been discussed and suggested to overlap with the adventitious carbon and hydroxyl peak (blue, 531.0 eV) [23], although it is difficult to distinguish here between a contribution from a satellite and a photoemission peak, and is instead assumed to be primarily adventitious species. This potentially overestimates the amount of adventitious contamination present when the rutile structure is formed, but this overestimation is expected to be negligible. Additionally, a new peak appears 0.8 eV below the O–Ru peak which is attributed to coordinatively unsaturated (cus) O–Ru (pink, 528.7 eV) [26]. Over *et al* suggest that either bridging (O_{br}) or on-top O atoms are represented by this cus O–Ru peak, based on DFT calculations that exhibit −1.07 eV and −0.86 eV energy shifts, respectively, relative to the lattice O peak. Once the sample is cooled to 70 °C (iterations 300–310), the adsorbed carbon and water return as their representive peaks increase, while the cus O–Ru peak decreases.

Table 1 displays the atomic ratios obtained from quantitative XPS analysis of the data from figure 2, representing the coverage of oxygen and carbon at the indicated temperatures. More about the atomic ratio calculations are provided in section S3 of the SI. Initially at RT (iterations 2–24), we see a significant amount of carbon coverage purely based on the

Table 1. Quantitative XPS atomic ratios for oxygen to total Ru atoms (O:Ru), carbon to total Ru atoms (C:Ru), and the ratio of Ru–O to Ru metal in the Ru 3d spectra (Ru–O:Ru^0). The O:Ru and C:Ru values represent the ML coverage for oxygen and carbon, respectively. The O:Ru value for 390 °C (marked with a star symbol) represents the stoichiometry of oxygen to Ru calculated based on the assumption of a rutile phase.

	250 °C [It. 90–110]	350 °C [It. 140–145]	390 °C [It. 210–250]
O:Ru	0.75	2.0	2.1*
C:Ru	1.7		0.6
Ru–O:Ru^0	0.8	1.3	

XPS intensities from figure 2, therefore we did not estimate the O or C coverage for this region as the attenuation through unknown carbon species complicates the calculation, rendering the overlayer model invalid. At 250 °C (iterations 90–110), when considering primarily chemisorbed oxygen, we calculate an O coverage of 0.75 ML. This value represents the ratio of the 'O–Ru' O 1s component to the total Ru 3d intensity minus the C 1s intensity, corrected for sensitivity based on the inelastic mean free path, interlayer distance, and respective differential photoabsorption cross sections. Because of the presence of residual water vapor and hydrogen in the high pressure cell, we did not include the total O 1s intensity in this calculation and instead just the peak known to be attributed to O–Ru. Alternatively, if we use the overlayer model to calculate the ratio of Ru–O:Ru^0 from the Ru 3d spectra using equation SE5 (SI) where we use the interlayer distance to correct for the attenuation seen only by Ru^0 electrons, we get a similar value of 0.8 ML. We speculate at this point that the Ru(0001) surface is covered with an incomplete monolayer of chemisorbed (1 × 1)-O that is reacting with the residual gases in the cell, therby creating a structure in-between a (2 × 1)-O and (1 × 1)-O overlayer, providing a coverage above 0.5 ML expected for the (2 × 1)-O layer, but also below 1 ML expected for the (1 × 1)-O layer [25]. Moreover, at 250 °C we see a peak energy difference of 0.54 eV between the Ru^0 and Ru–O, which is most consistent with the (2 × 1)-O layer [25, 26].

After further annealing to 350 °C, we can still apply the overlayer model as the overlayer thickness is not expected to be more than the interlayer thickness and thus has negligible attenuation of substrate photoelectrons. Unlike for the 250 °C spectra, we are unable to fit a C 1s peak in the spectra after constraining the binding energy difference and intensity ratio provided by the Ru 3d spin-orbit splitting. Since the O 1s component is primarily O–Ru, we used the total O 1s signal relative to the Ru 3d intensity to calculate a coverage of 2 ML, which strongly suggests the formation of a O–Ru–O trilayer terminating the surface. We can recalculate this coverage by accounting for the attenuation through the expected trilayer using the proposed model from DFT calculations provided in [15]. Equations SE8 and SE9 provided in the SI use the interlayer distances provided for the '2 ML fcc/tetra-I trilayer model' [15], which allow us to calculate a more accurate atomic density ratio with equation SE6. As the number of layers (n) of Ru atoms in equation SE8 approaches infinity,

the model then represents a trilayer on top of a bulk Ru(0001) substrate. After $n =$ nine layers, the change in the O:Ru ratio for subsequent layers is negligible (<0.01) and converges at 2.3 ML. While not in complete agreement with the overlayer model, this excess O is likely due to the presence of water on the surface. We also note that the Ru3d$_{5/2}$ spectra show a similar shape as a high-resolution spectra for ∼2 ML of oxygen on Ru(0001) in [13], suggesting that the trilayer is also stable at RT under UHV conditions. It was proposed by Reuter *et al* that following the formation of a surface trilayer, intercalation of oxygen should take place forming a so called floating trilayer [15]. Unfortunately, we do not see any strong evidence for stable formation of multiple trilayers based on our quantitative analysis. Additionally, for such a floating trilayer, the O1s BE should shift by 1.1 eV (calculated by DFT) and almost coincide with the O1s levels of the RuO_2(110) domains [15], which we also do not observe here in figure 1(a) or figure 2(b).

Once the transition to RuO_2 has taken place at 390 °C, the formed rutile structure must be considered for the atomic ratio calculations. Initial values using the same parameters for the previously used ultrathin overlayer model yielded O:Ru values of <0.2, which chemically does not make sense. To obtain more accurate values a correction factor was used similar to what was used for the trilayer structure above and is briefly described in section S3 in the SI, and more detailed in the SI of [29]. The O:Ru ratio was calculated based on an assumed probing depth of $3\lambda\left(E_{\mathrm{kin}}^{\mathrm{Ru-RuO_2}}\right)$ (∼2.6 nm) which corresponds to roughly $n = 8$ layers and is expected to be less than the formed RuO_2 film thickness. We additionally calculated the ratio with up to $n = 15$ layers, however the change in O:Ru for additional layers was negligible (<0.01) and converged to a O:Ru ratio of 2.1. This is close to the expected value for rutile RuO_2(110) which is suggested to be formed based on the measured XPS binding energies. With an interlayer distance of $d_{\perp,\mathrm{RuO2}} = 3.2$ Å [30], $n = 8$ layers equates to a thickness of approximately 2.6 nm, which is reasonably close to previous studies of Ru thermal oxidation under similar conditions (300 °C–350 °C, $p_{O2} = 10^{-5} - 10^{-1}$ mbar) yielding a thickness of 1.6 nm based on surface x-ray diffraction measurements [30], although thickness is expected to vary based on exposure time and temperature. This thickness is also fully consistent with the complete loss of the Ru^0 component seen in the Ru 3d spectra.

After cooling to 70 °C we see in figure 2(b) that the carbon and hydrogen related components of the O 1s peak increases strongly. However, the uptake of adsorbed carbon and water during cooling increases the contribution from contamination, resulting in overestimating the O thickness. Like for the initial RT spectra, we did not estimate the adventitious O or C coverages for this region.

In addition to the reported isobaric experiment, we conducted an isothermal experiment where the temperature was held at 390 °C and the pressure was increased from a base pressure of 1×10^{-7} mbar to $p_{O2} = 6 \times 10^{-3}$ mbar. Figure S10 in the SI shows heat maps of the O 1s (a) and Ru 3d (b) core levels, along with a plot showing the pressure versus time during APXPS measurements. Spectra collection started once the $p_{O2} = 1 \times 10^{-3}$ mbar until $p_{O2} = 6 \times 10^{-3}$ mbar, which took approximately 45 min. Initially, we see a clean sample with no visible peak in the O 1s spectra. After an initial uptake of pressure to $p_{O2} = 5 \times 10^{-3}$ mbar, corresponding to the 15 min mark, we see the formation of a peak at 529.5 eV that stays constant for the remainder of the experiment. In the Ru 3d spectra, a slight change in intensity occurs at approximately 11 min, followed by the formation of a shoulder at 281 eV after 19 min, corresponding to Ru–O. Unfortunately, due to the instability of the leak valve in this pressure range, the speed of the reaction with respect to pressure was too fast to detect any intermediate oxidation states.

Following oxidation, LEED and XPD were used *ex situ* in a different UHV system to verify the crystallinity and the crystal structure of the formed RuO_2 oxide. The samples used for both LEED and XPD were part of the same wafer that was pretreated with a 600 °C anneal used for APXPS measurements but were oxidized and characterized separately in a different chamber due to lack of LEED capability at the APXPS endstation. A brief LEED analysis is provided in the SI. Figure 3 shows the measured Ru 3d$_{5/2}$ XPD patterns from the grown RuO_2 film (a) and the pristine Ru(0001) substrate (c), as well as the O 1s XPD pattern from the oxide film in (b). The RuO_2(110) surface contains no three-fold symmetry, unlike Ru(0001) which has p3m1-hexagonal symmetry. Instead, RuO_2(110) has pmm-rectangular symmetry, which means that applying a rotation of 180° leaves the measured XPD pattern unchanged. This two-fold symmetry is readily observed when simulating the Ru 3d$_{5/2}$ XPD pattern from a RuO_2(110) cluster, as shown in figure S3 of the SI. However, the XPD data from a thermally grown RuO_2(110) film show six-fold rather than a two-fold symmetry, as three domains of RuO_2(110) oriented at 0°, 120° and 240° with respect to each other form on the Ru(0001) surface. Three-folding the simulated XPD data shown in figure S3 and aligning it with the substrate orientation as depicted in figure 3(f), we obtain the simulated patterns (d) and (e) for Ru 3d$_{5/2}$ and for O 1s, respectively. The agreement with the corresponding experimental data is satisfactory and confirms our structural assignment. Defects such as RuO_2 domain boundaries are obviously not included in the simulated XPD spectra. Further details of the XPD analysis and simulated data are provided in the SI.

The orientation of the oxide domains relative to the substrate can thus be determined. The [001] direction of the oxide aligns with the [1000] direction of the substrate, while the [1$\bar{1}$0] direction points towards the [01$\bar{1}$0] direction of the substrate. This agrees with the oxide/substrate orientation given by Kim *et al* [31] Also, the LEED image depicted in the figure S2(b) is consistent with the alignment determined by the XPD measurements.

In summary, we provide spectral evidence for the formation of a O–Ru–O trilayer structure during thermal oxidation of Ru(0001) as a precursor towards the formation of

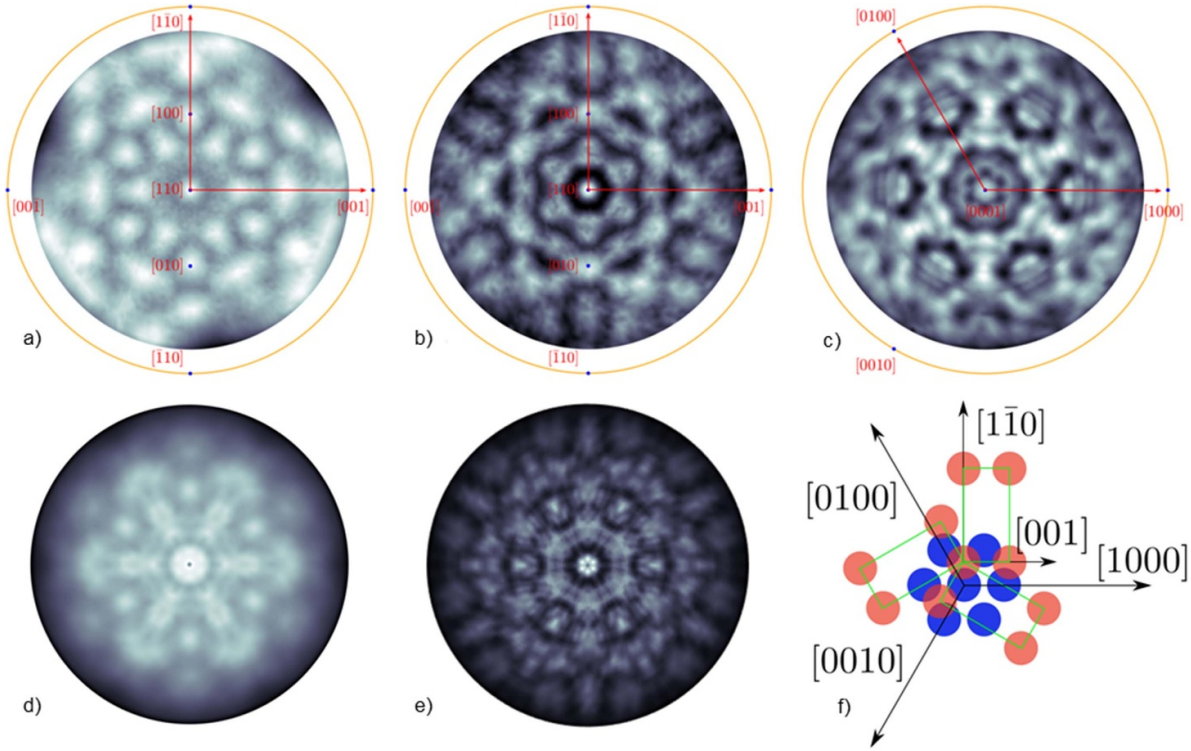

Figure 3. Measured XPD patterns of (a) the Ru $3d_{5/2}$ peak from the $RuO_2(110)$ oxide layer on the Ru(0001) substrate measured at 973 eV kinetic energy, (b) the O 1s peak from the same sample taken at 1210 eV kinetic energy (O 1s), and (c) the Ru $3d_{5/2}$ from a clean Ru(0001) film collected at 973 eV kinetic energy. Measured Ru data (a), (c) were taken with Mg Kα radiation (1253.6 eV photon energy), while measured O data (b) were taken with Si Kα radiation (1739.5 eV photon energy). All measured data are processed by three-fold averaging and Laplace filtering. The polar angle range is from 0° to 82° in all data. Low index directions are indicated. Corresponding XPD patterns simulated with a $RuO_2(110)$ cluster are given for Ru $3d_{5/2}$ emission at 973 eV (d) and for O 1s emission at 1210 eV (e) kinetic energy. The used cluster size was $N = 1272$ atoms (see cluster model in SI figure S4). The adsorption geometry unit vectors of the oxide film overlaid with the substrate is depicted in (f).

rutile $RuO_2(110)$, as well as the structural characterization of the grown RuO_2 thin film. Initially during oxidation, oxygen adsorbs to the clean Ru(0001) surface, where the surface coverage is strongly dependent on the O_2 partial pressure and temperature. Lower temperatures (<130 °C) and pressures ($<10^{-5}$ mbar) generally form 1 ML coverages consistent with a (1 × 1) structure [4, 13]. For higher temperatures (>130 °C) and pressures ($>10^{-4}$ mbar), oxygen is incorporated below the surface and forms a 2 ML surface oxide, as evidenced from our results. The thickness and stoichiometry are compatible with the fcc/tetra-I 2 ML trilayer structure proposed by Reuter *et al* [15] Once this metastable trilayer structure forms, a rapid autocatalytic oxidation occurs towards the rutile $RuO_2(110)$ structure. Similar oxidation behavior has recently been demonstrated for Ir(100) [29]. The formation of stacked O–Ru–O trilayers with thicknesses of 3–4 trilayers is the proposed precursor [15] that should form immediately after the 2 ML trilayer as more oxygen is intercalated into the lattice. However, our time-resolved experiment was unable to provide conclusive evidence of this structure, likely due to the speed of the structural transition. Our structural characterization with XPD and LEED provides good agreement with the rutile $RuO_2(110)$ structure, therefore we do not believe the quality or thickness of our single-crystalline Ru(0001) films played any role in our ability to detect other precursors. Ultimately, our results provide valuable information for better understanding the oxidation of Ru(0001) and demonstrate the strength of time-lapsed APXPS and the combination with XPD towards investigating surface transformation mechanisms and structural characterization, respectively.

4. Conclusions

We have used time-lapsed APXPS to identify potential metastable precursors that form during the thermal oxidation of Ru(0001) toward $RuO_2(110)$. From XPS peak energy analysis, we show that initially an O overlayer is formed, followed by a O–Ru–O trilayer structure, before a rapid transition to rutile $RuO_2(110)$ occurs. This pathway agrees well with previously proposed theoretical models and provides spectral evidence for a metastable precursor required for full oxidation of Ru(0001) to $RuO_2(110)$. Quantitative analyses of XPS intensities using DFT calculated models from prior literature for the trilayer and rutile structure agree well with our proposed pathway concluded from the analysis of binding energies. We were unable to obtain spectral evidence for a 'floating' trilayer, which was proposed to form once the initial trilayer has been established and before transitioning into rutile $RuO_2(110)$. We

then provide XPD measurements for a RuO_2(110) film grown on Ru(0001) through thermal oxidation, showing good agreement with simulated RuO_2(110) models and confirming that a rutile structure was formed.

Data availability statement

The data that support the findings of this study are available upon reasonable request from the authors.

Acknowledgments

This work was performed at the *In Situ* Spectroscopy (X07DB) beamline of the Swiss Light Source, Paul Scherrer Institut, Villigen PSI, Switzerland, using the Solid−Gas Interface Chamber (SGIC). We acknowledge the support at the SGIC endstation and ISS beamline provided by Dr Luca Artiglia and Dr Jörg Raabe, and we thank Dr Matthias Schreck and Dr Michael Weinl for making the Ru(0001) film samples available to us. This research was funded by the Swiss National Science Foundation via the project grant 200020_172641 and by the European Union's Horizon 2020 programme (FP-RESOMUS-MSCA 801459).

Author contributions

The manuscript was written through contributions of all authors. All authors have given approval to the final version of the manuscript.

ORCID iDs

J Trey Diulus https://orcid.org/0000-0001-8675-8581
Jürg Osterwalder https://orcid.org/0000-0001-9517-641X
Zbynek Novotny https://orcid.org/0000-0002-3575-7535

References

[1] Cui X, Zhou J, Ye Z, Chen H, Li L, Ruan M and Shi J 2010 Selective catalytic oxidation of ammonia to nitrogen over mesoporous CuO/RuO_2 synthesized by co-nanocasting-replication method *J. Catal.* **270** 310–7
[2] Seki K 2010 Development of RuO_2/rutile-TiO_2 catalyst for industrial HCl oxidation process *Catal. Surv. Asia* **14** 168–75
[3] Liu H and Iglesia E 2005 Selective oxidation of methanol and ethanol on supported ruthenium oxide clusters at low temperatures *J. Phys. Chem.* B **109** 2155–63
[4] Over H 2012 Surface chemistry of ruthenium dioxide in heterogeneous catalysis and electrocatalysis: from fundamental to applied research *Chem. Rev.* **112** 3356–426
[5] Lundgren E, Mikkelsen A, Andersen J N, Kresse G, Schmid M and Varga P 2006 Surface oxides on close-packed surfaces of late transition metals *J. Phys.: Condens. Matter* **18** R481–99
[6] Over H, Seitsonen A P, Lundgren E, Schmid M and Varga P 2001 Direct imaging of catalytically important processes in the oxidation of CO over RuO_2(110) *J. Am. Chem. Soc.* **123** 11807–8
[7] Böttcher A, Starke U, Conrad H, Blume R, Niehus H, Gregoratti L, Kaulich B, Barinov A and Kiskinova M 2002 Spectral and spatial anisotropy of the oxide growth on Ru(0001) *J. Chem. Phys.* **117** 8104–9
[8] Over H 2000 Atomic-scale structure and catalytic reactivity of the RuO_2(110) surface *Science* **287** 1474–6
[9] Farfan-Arribas E and Madix R J 2002 Role of defects in the adsorption of aliphatic alcohols on the TiO_2(110) surface *J. Phys. Chem.* B **106** 10680–92
[10] Kulkarni D and Wachs I E 2002 Isopropanol oxidation by pure metal oxide catalysts: number of active surface sites and turnover frequencies *Appl. Catal. A Gen.* **237** 121–37
[11] Blume R, Niehus H, Conrad H, Böttcher A, Aballe L, Gregoratti L, Barinov A and Kiskinova M 2005 Identification of subsurface oxygen species created during oxidation of Ru(0001) *J. Phys. Chem.* B **109** 14052–8
[12] Blume R, Niehus H, Conrad H and Böttcher A 2004 Oxide-free oxygen incorporation into Ru(0001) *J. Chem. Phys.* **120** 3871–9
[13] Knop-Gericke A *et al* 2009 Chapter 4 X-ray photoelectron spectroscopy for investigation of heterogeneous catalytic processes *Advances in Catalysis* vol 52 (Amsterdam: Elsevier) pp 213–72
[14] Over H 2002 Oxidation of metal surfaces *Science* **297** 2003–5
[15] Reuter K, Ganduglia-Pirovano M V, Stampfl C and Scheffler M 2002 Metastable precursors during the oxidation of the Ru(0001) surface *Phys. Rev.* B **65** 165403
[16] Over H, Seitsonen A P, Lundgren E, Smedh M and Andersen J N 2002 On the origin of the Ru-$3d_{5/2}$ satellite feature from RuO_2(110) *Surf. Sci.* **504** L196–200
[17] Gsell S, Fischer M, Schreck M and Stritzker B 2009 Epitaxial films of metals from the platinum group (Ir, Rh, Pt and Ru) on YSZ-buffered Si(111) *J. Cryst. Growth* **311** 3731–6
[18] Watts B, Pilet N, Sarafimov B, Witte K and Raabe J 2018 Controlling optics contamination at the PolLux STXM *J. Instrum.* **13** C04001
[19] Greber T, Raetzo O, Kreutz T J, Schwaller P, Deichmann W, Wetli E and Osterwalder J 1997 A photoelectron spectrometer for *k*-space mapping above the Fermi level *Rev. Sci. Instrum.* **68** 4549–54
[20] Orlando F *et al* 2016 The environmental photochemistry of oxide surfaces and the nature of frozen salt solutions: a new *in situ* XPS approach *Top. Catal.* **59** 591–604
[21] Raabe J *et al* 2008 PolLux: a new facility for soft x-ray spectromicroscopy at the Swiss Light Source *Rev. Sci. Instrum.* **79** 113704
[22] De Abajo F J G, Van H M A and Fadley C S 2001 Multiple scattering of electrons in solids and molecules: a cluster-model approach *Phys. Rev.* B **63** 075404
[23] Morgan D J 2015 Resolving ruthenium: XPS studies of common ruthenium materials *Surf. Interface Anal.* **47** 1072–9
[24] Chan H Y H, Takoudis C G and Weaver M J 1997 High-pressure oxidation of ruthenium as probed by surface-enhanced Raman and x-ray photoelectron spectroscopies *J. Catal.* **172** 336–45
[25] Lizzit S *et al* 2001 Surface core-level shifts of clean and oxygen-covered Ru(0001) *Phys. Rev.* B **63** 205419
[26] Over H, Seitsonen A P, Lundgren E, Wiklund M and Andersen J N 2001 Spectroscopic characterization of catalytically active surface sites of a metallic oxide *Chem. Phys. Lett.* **342** 467–72
[27] Kim Y J, Gao Y and Chambers S A 1997 Core-level X-ray photoelectron spectra and X-ray photoelectron diffraction of RuO_2(110) grown by molecular beam epitaxy on TiO_2(110) *Appl. Surf. Sci.* **120** 250–60
[28] Knapp M, Crihan D, Seitsonen A P, Resta A, Lundgren E, Andersen J N, Schmid M, Varga P and Over H 2006

Unusual process of water formation on RuO_2(110) by hydrogen exposure at room temperature *J. Phys. Chem.* B **110** 14007–10

[29] Novotny Z, Tobler B, Artiglia L, Fischer M, Schreck M, Raabe J and Osterwalder J 2020 Kinetics of the thermal oxidation of Ir(100) toward IrO_2 studied by ambient-pressure x-ray photoelectron spectroscopy *J. Phys. Chem. Lett.* **11** 3601–7

[30] He Y B, Knapp M, Lundgren E and Over H 2005 Ru(0001) model catalyst under oxidizing and reducing reaction conditions: *in-situ* high-pressure surface x-ray diffraction study *J. Phys. Chem.* B **109** 21825–30

[31] Kim Y D, Schwegmann S, Seitsonen A P and Over H 2001 Epitaxial growth of RuO_2(100) on Ru(10$\bar{1}$0): surface structure and other properties *J. Phys. Chem.* B **105** 2205–11